

Computational modeling of dynamic mechanical properties of pure polycrystalline magnesium under high loading strain rates

Qizhen Li^{1,2,a}

¹School of Mechanical and Materials Engineering, Washington State University, Pullman, WA 99164, USA

²Department of Chemical and Materials Engineering, University of Nevada, Reno, Reno, Nevada 89557, USA

Abstract. Computational simulations were performed to investigate the dynamic mechanical behavior of pure polycrystalline magnesium under different high loading strain rates with the values of 800, 1000, 2000, and 3600 s⁻¹. The Johnson-Cook model was utilized in the simulations based on finite element modeling. The results showed that the simulations provided well-matched predictions of the material behavior such as the strain rate-time history, the stress-strain curve, and the temperature increase. Under high loading strain rates, the tested material experienced linear strain hardening at the early stage of plastic deformation, increased strain hardening at the intermediate plastic deformation region, and decreased strain hardening at the region before fracture. The strain hardening rates for the studied high loading strain rate cases do not vary much with the change of strain rates.

1. Introduction

As the lightest structural metal, magnesium is an attractive material candidate for various structural components in automobiles, aircrafts, etc.. These components often experience high strain rate dynamic loadings during their actual service. Thus, research efforts were devoted to study dynamic mechanical properties of magnesium and its alloys such as ZK60, Mg-Gd-Y, AZ80, AZ31, magnesium single crystal, and pure polycrystalline magnesium [1–6].

The experimental investigations require a split Hopkinson pressure bar (SHPB) system and it can be costly. Therefore, it is often appealing to investigate the dynamic mechanical properties through computational simulations. To achieve meaningful simulations, appropriate theoretical models are needed. Among the theoretical models for high strain rate loading conditions, the Zerilli-Armstrong model [7–10] and the Johnson-Cook model [11, 12] are the most commonly used because of their simple forms. The model's simplicity can result in the save of computational resources.

This study performed computational simulations of mechanical behavior of pure polycrystalline magnesium under a range of high loading strain rates using finite element method. The loading strain rates are chosen to be the same as those experimental strain rates in the reference [6]. The simulation results were compared with the experimental data for validation.

2. Computational method and data analysis

ABAQUS\Explicit is utilized for three-dimensional modeling of high strain rate tests. To be the same as the experimental SHPB set-up as shown in the schematic

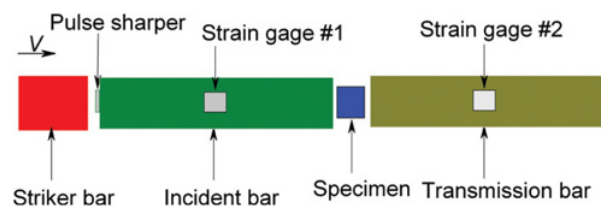


Figure 1. Schematic drawing of a SHPB system. The striker bar applies the loading stress wave, the specimen is held between the incident bar and the transmission bar, and strains are measured using strain gauges #1 and #2.

drawing in Fig. 1, aluminum is chosen to be the material used for the striker, incident, and transmission bars. Eight-node solid elements are used for the bars and samples in the simulations. The bars are assumed to behave elastically. The Johnson-Cook model was implemented in the modeling. Simulations are performed for the same strain rates as the reference [6]: 800, 1000, 2000, and 3600 s⁻¹.

When performing a high strain rate testing with a SHPB system, the striker bar is first accelerated to a certain velocity V , then it hits the incident bar to generate an incident stress wave in this incident bar. This stress wave has $\sigma = \rho CV/2$, where C is the wave speed and $C = \sqrt{E/\rho}$. ρ and E are the density and Young's modulus of the bar. Since aluminum is used for the bars, the Young's modulus E is 75 GPa, the density ρ is 2700 kg/m³, and the speed C of the stress wave is ~ 5270 m/s. The collected data are the incident strain $\varepsilon_I(t)$, the reflected strain $\varepsilon_R(t)$, and the transmission strain $\varepsilon_T(t)$. These three strains are functions of testing time, and the summation of the absolute reflected strain and the absolute transmission strain equals to the absolute incident strain, i.e. $|\varepsilon_I(t)| = |\varepsilon_R(t)| + |\varepsilon_T(t)|$. These collected strains are employed to compute the high strain rate dynamic stress $\sigma(t)$, strain $\varepsilon(t)$,

^a Corresponding author: Qizhen.Li@wsu.edu

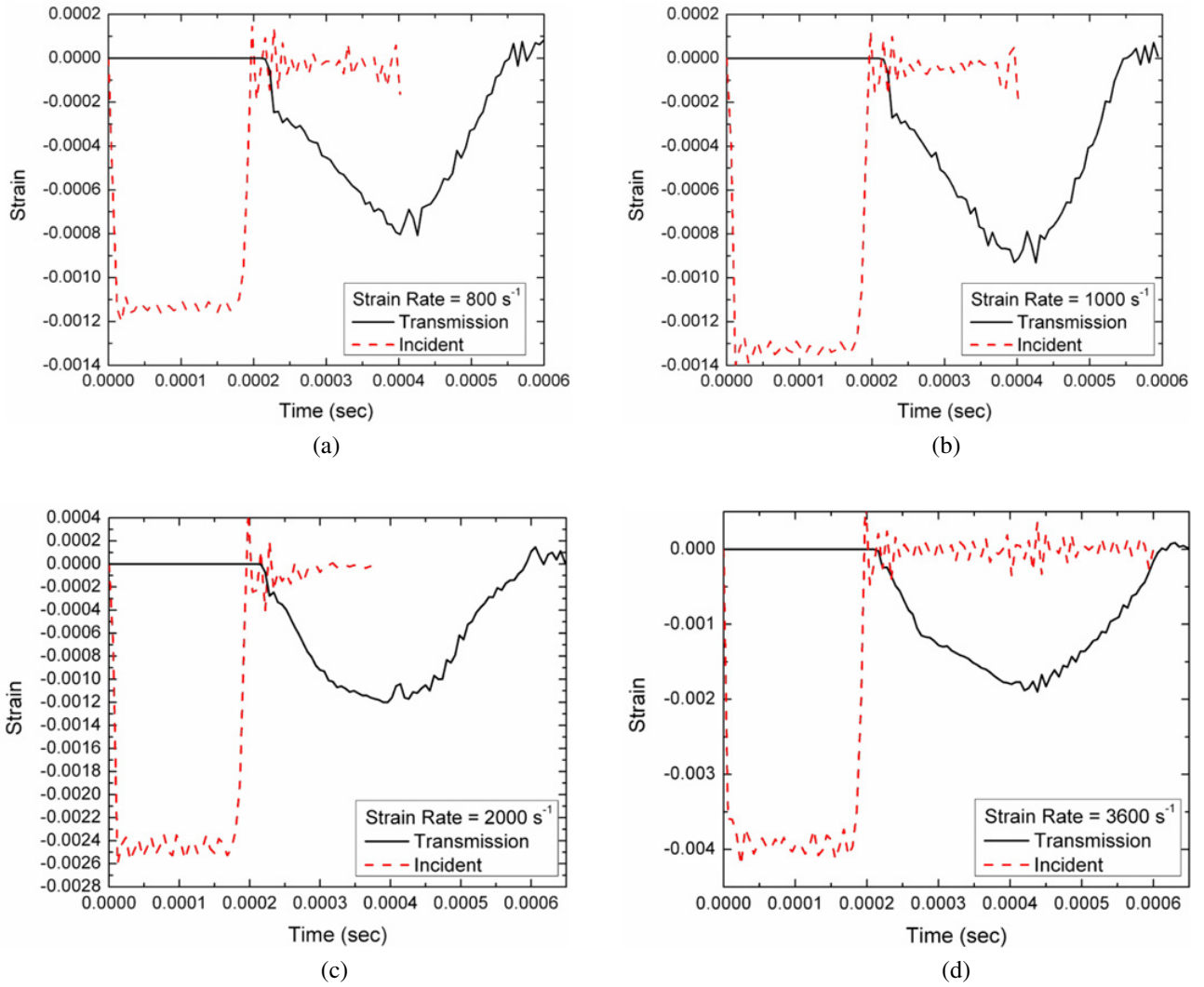


Figure 2. Strain-time histories of the incident strain and the transmission strain for different high strain rates. (a) 800 s^{-1} ; (b) 1000 s^{-1} ; (c) 2000 s^{-1} ; (d) 3600 s^{-1} . Note: the incident strain is the dashed curve and the transmission strain is the solid curve for each strain rate case.

and strain rate $\dot{\varepsilon}(t)$ based on one-dimensional wave theory [13] as follows.

$$\sigma(t) = \frac{EA_0}{A} \varepsilon_T(t) \quad (1)$$

$$\varepsilon(t) = -\frac{2C}{L} \int_0^t \varepsilon_R(t) dt \quad (2)$$

$$\dot{\varepsilon}(t) = \frac{d\varepsilon}{dt} = -\frac{2C}{L} \varepsilon_R(t). \quad (3)$$

Where A_0 , A , and L are the cross-section area of the bar, the cross-section of the specimen, and the original length of the specimen.

3. Results and discussions

Simulations were performed for the four loading strain rate cases: 800 , 1000 , 2000 , and 3600 s^{-1} . These four strain rates were chosen because they were employed in the

experimental testing reported in the reference [6]. For each of the four strain rates simulated in this work, the incident strain $\varepsilon_I(t)$ and the transmission strain $\varepsilon_T(t)$ were extracted from the incident and transmission bars and reported in Fig. 2.

Figure 3 reports the strain rate versus time curves from experimental testing and finite element modeling for different strain rates (800 , 1000 , 2000 , and 3600 s^{-1}). The experimental curves show (a) the strain rate fluctuation with time; (b) the higher the strain rate is, the shorter the testing time is; and (c) the strain rate reaches a peak value early in a test and then diminishes slightly as the test continues. The computational curves show that the strain rate reaches the nominal value faster than the experimental curves. This may be due to the inertia of deformation process corresponding to the real experiments. For all the tested strain rates, the strain rate drops after reaching a maximum value. This relates to the strain waves propagating in the incident and transmission bars. As shown in Fig. 2, a constant-amplitude incident strain or stress pulse is generated by the striking bar;

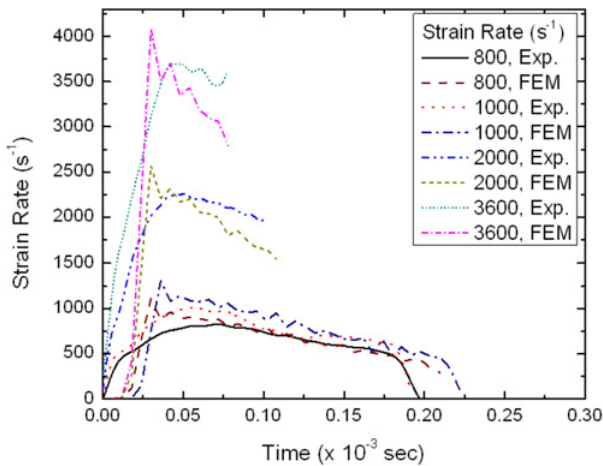


Figure 3. Strain rate versus time for the studied dynamic tests with strain rates of 800, 1000, 2000, and 3600 s^{-1} , at room temperature from experimental testing and finite element modeling.

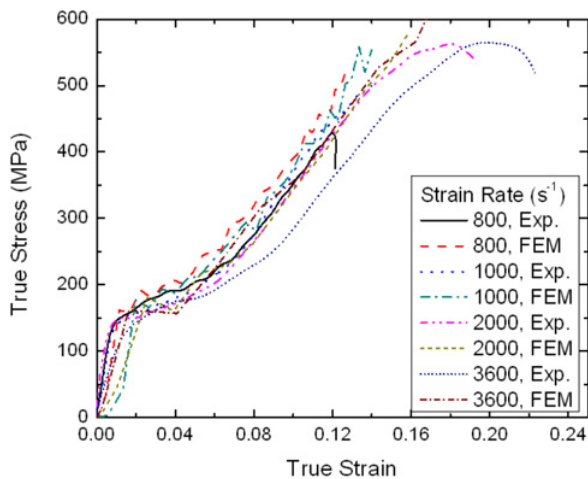


Figure 4. True stress-true strain curves for the strain rates of 800, 1000, 2000, and 3600 s^{-1} from experimental testing and finite element modeling.

this pulse is partially transmitted and partially reflected. The summation of the transmitted and reflected pulses equals to the incident pulse. The figures show that the transmitted pulse is not constant, thus the reflected pulse is also not constant. According to Eq. (3), the reflected pulse is proportional to the strain rate. Thus, the strain rate is not constant, which is true to both experimental and simulated data. These data reported in Fig. 2 are employed to calculate the stress-strain curves for all the cases. The computed stress-strain curves are reported in Fig. 4. To make a comparison with the experimental testing, the experimental stress-strain curves for all high strain rate cases are also included in Fig. 4. The results show that the stress-strain curves of the material from the modeling match the experimental curves.

The temperature increase (ΔT) for each dynamic strain rate can be computed. It is known that most of the work during the high strain rate testing is converted to heat. In the simulations, the fraction of energy converted to heat is

assumed to be 90%. The temperature increases can also be calculated from the experimental stress-strain curves and the values are 15.0, 19.0, 32.4, and 38.2 K for the strain rates of 800, 1000, 2000, and 3600 s^{-1} respectively. The temperature changes are 15.0, 19.0, 32.4, and 38.2 K from the modeling for the strain rate of 800, 1000, 2000, and 3600 s^{-1} respectively. The predictions of ΔT by finite element modeling match those from experimental data.

4. Conclusion

Dynamic mechanical behaviour of pure polycrystalline magnesium samples were simulated using finite element method. The loading strain rates were chosen to be 800, 1000, 2000, and 3600 s^{-1} to compare with the reported experimental data [6]. Overall, the simulations provided well-matched predictions of the material behavior such as the strain rate-time history, the stress-strain curve, and the temperature increase. The high strain rate responding features were captured by the computational modeling. The dynamic stress-strain curves show linear strain hardening at the early stage of plastic deformation, increased strain hardening at the intermediate plastic deformation region, and decreased strain hardening at the region before fracture. The strain hardening rates for the cases with the studied high loading strain rates have negligible variation when the strain rates vary in the range of 800–3600 s^{-1} . Computational modeling is very useful for obtaining material properties under different loading strain rates while reducing the cost for performing actual experimental tests.

The support for the research from the national science foundation under DMR-1449607 and the US Department of Energy, Office of Basic Energy Sciences under Grant No. DE-SC0002144 is greatly appreciated.

References

- [1] Y. Fan, Q. Wang, J. Ning, J. Chen, W. Ji, *Journal of Applied Mechanics* **77**, 051902, 77 (2010).
- [2] E. El-Magd, and M. Abouridouane, *International Journal of Impact Engineering* **32**, 741 (2006).
- [3] Q.Z. Li, *Journal of Applied Physics* **109**, 103514 (2011).
- [4] Q.Z. Li, *Materials Science and Engineering A* **568**, 96 (2013).
- [5] M.T. Tucker, M.F. Horstemeyer, P.M. Gullett, H.E. Kadiri, W.R. Whittington, *Scripta Materialia* **60**, 182 (2009).
- [6] Q.Z. Li, *Materials Science and Engineering A* **540**, 130 (2012).
- [7] F.J. Zerilli, R.W. Armstrong, *Acta Metallurgica et Materialia* **40(8)**, 1803 (1992).
- [8] F.J. Zerilli, R.W. Armstrong, *Journal of Applied Physics* **61(5)**, 1816 (1987).
- [9] F.J. Zerilli, R.W. Armstrong, *Journal de Physique IV* **49(C3)**, 529 (1988).

- [10] R.W. Armstrong, Q.Z. Li, Metallurgical and Materials Transactions A, 2015, DOI: 10.1007/s11661-015-2779-6
- [11] G.R. Johnson, W.H. Cook, 7th international Symposium on Ballistics, Hague, Netherlands 541 (1983).
- [12] G.R. Johnson, W.H. Cook, Engineering Fracture Mechanics **21**, 31 (1985).
- [13] H.E. Boyer, and T.L. Gall, Metals handbook (9th ed.), American Society for Metals, Materials Park (OH) 190 (1985).